Short Papers

Evaluation of Telerobotic Shared Control Strategy for Efficient Single-Cell Manipulation

Jungsik Kim, Hamid Ladjal, David Folio, Antoine Ferreira, *Member, IEEE*, and Jung Kim, *Member, IEEE*

***Abstract*—Microinjection is a method for the delivery of exogenous materials into cells and is widely used in biomedical research areas such as transgenics and genomics. However, this direct injection is a time-consuming and laborious task, resulting in low throughput and poor reproducibility. Here, we describe a telerobotic shared control framework for microinjection, in which a micromanipulator is controlled by the shared motion commands of both the human operator and the autonomous controller. To determine the weightings between the operator and the controller, we proposed a quantitative evaluation method using a model of speed/accuracy trade-offs in human movement. The results showed that a 40%–60% weighting on the human operator (or the controller) produced the best performance for both speed and accuracy of guiding and targeting task in microinjection suggesting that some level of both automation and human involvement is important for microinjection tasks.**

***Note to Practitioners*—In single-cell microinjection, for the small size and delicate structure of a cell, to date, most human operators have manipulated biological cells manually; therefore, low manipulation efficiency and poor reproducibility has been reported for this task. Most manipulation systems have primarily focused on limited visual feedback in conjunction with a dial-based console system, requiring extensive operator training to perform injection tasks with reproducible results. To address these problems, a telerobotic shared control method for microinjection was developed by integrating the automatic and direct manipulation functions of a robotic system. While a controller retains cells and glass pipettes within a desired path or space, the operator can concentrate on the injection task, thus achieving high throughput and dexterity.**

***Index Terms*—Fitts' and steering laws, microrobotic control, single-cell microinjection, telerobotic shared control.**

I. Introduction

The highly efficient transfer of foreign materials into cells remains a challenge in biotechnology, both for fundamental cellular and molecular biology research and in biomedicine. Several methods have been developed for the successful delivery of exogenous materials into cells. Among them, single-cell microinjection is performed to directly introduce foreign materials, such as DNA, proteins, sperm and drugs, into individual cells [1]–[3]. The efficiency in microinjection can be classified as delivery and manipulation efficiencies. The delivery efficiency is associated with the successful transfer and the manipulation efficiency means the degree of easiness to manipulate cells. Although microinjection has relatively high delivery efficiencies than electrical [4], viral [1], chemical [1], and other transfer methods [5], [6], the injection task is time-consuming and labor-intensive work that limits the manipulation of large numbers of single cells [1], [2]. In addition, great manipulation skills are required of a human operator requiring extensive training to perform these injection tasks; thus, microinjection has low manipulation efficiencies, resulting in low throughput and poor reproducibility.

Several single-cell microinjection systems have been proposed to improve the manipulation efficiency. Automated microinjection systems have been developed to remove human involvement from the injection process [7]–[10], where a visual servoing approach is usually used to control the position and force of a micromanipulator; however, it is challenging to create a fully automated system because microinjection is conducted under diverse and complex conditions such as varying cell size (from one micrometer to hundreds of micrometers), cell types (e.g., suspended or attached ones) and liquid mediums. Therefore, there are difficulties in the dexterous manipulation of cells with multiple degrees of freedom (DOF) and in target selection (e.g., cell nucleus or cytoplasm) in visual servoing [11]–[13]. Teleoperated microinjection systems have been developed to provide haptic feedback during manipulation [14]–[16]. However, most of them have provided force sensing and feedback for only a small number of DOF.

Here, we present a telerobotic shared control (TSC) framework developed for single-cell microinjection with high manipulation efficiency. The motivation of the TSC arose from the idea that the collaboration of a human and a robotic system can increase the quality and capability of manipulation by exploiting a human's ability to skillfully manipulate objects with dexterity and disturbance adaptation along with a robot's accuracy and repeatability [17], [18]. To reduce the difficulties in biomicromanipulation mentioned above and simultaneously achieve high throughput and dexterity, both automatic and direct manipulation functions of the system are needed in microinjection. In the TSC approach, a human operator can control the manipulator as much as possible, while a controller retains cells and glass pipettes within a desired manipulation path or space to provide adequate performance.

In the remainder of this paper, toward the development of TSC for microinjection, the TSC strategy is first presented with focusing on the task guiding a glass pipette to a target position as a key procedure in the microinjection. In addition, we provide a quantitative analysis to determine what level of automation (or direct manipulation) is needed for TSC. Most previous studies on shared control have not addressed how to determine the degree of autonomy (or human involvement) to implement in the telemanipulation for the best performance. Although shared control has been applied to various applications [18], [19], this work is, to the authors' knowledge, the first providing an evaluation method for determining the optimal shared control gains and the first application of shared control in a cellular micromanipulation.

II. Method

A. Telerobotic Microinjection System Design

In a conventional microinjection task, attached and suspended cells can be injected. In this paper, we focused on the microinjection of suspended cells such as embryos. The microinjection task for suspended cells consists of: (i) the preparation of a injection pipette (focusing and

Manuscript received January 21, 2011; revised June 23, 2011; accepted October 23, 2011. Date of publication November 15, 2011; date of current version April 03, 2012. This paper was recommended for publication by Associate Editor S. Fatikow and Editor K. Goldberg upon evaluation of the reviewers' comments. This work was supported in part by Basic Science Research Program through the National Research Foundation of Korea (NRF) funded by the Ministry of Education, Science and Technology (2011-0026011).

J. S. Kim and J. Kim are with the Department of Mechanical Engineering, Korea Advanced Institute of Science and Technology, Daejeon, 305-701, Korea (e-mail: js_kim@kaist.ac.kr; jungkim@kaist.ac.kr).

H. Ladjal, D. Folio, and A. Ferreira are with the Laboratoire PRISME, ENSI de Bourges, 88 Boulevard de Lahitolle, 18020 Bourges, France (e-mail: hamid.ladjal@ensi-bourges.fr; david.folio@ensi-bourges.fr; antoine.ferreira@ensi-bourges.fr).

Digital Object Identifier 10.1109/TASE.2011.2174357

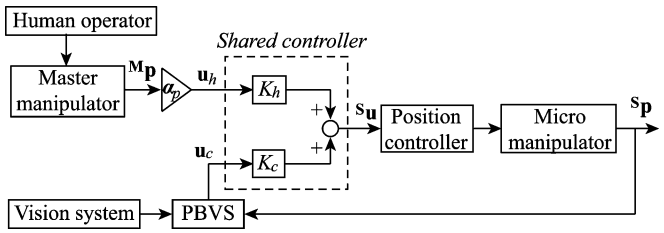

Fig. 1. TSC block diagram. Position-based visual servoing (PBVS) represents the artificial potential field in this paper, and position controller is a simple PID controller. $^{S}\mathbf{p}$ and $\mathbf{u}$ are in μm, and $^{M}\mathbf{p}$ is in mm.

filling); (ii) selection and holding of cells with a holding pipette; (iii) cellular orientation control; (iv) pipette insertion and injection of materials into cells; and (v) withdrawing a pipette. This paper focused on the TSC strategy for the injection task (step iv and v).

The telerobotic biomicromanipulation system for microinjection consists of a master robot to input the operator's motion command, micromanipulators with glass micropipettes and a microscopic vision system. The task space of the master robot is represented by the coordinate frame $\{\mathbf{M} : (x, y, z)\} \in \Re^3$, the task space of the micromanipulator is represented by the coordinate frame $\{\mathbf{S} : (X, Y, Z)\} \in \Re^3$, and the image space of the fixed camera is defined by the image coordinate frame $\{\mathbf{I} : (u, v)\} \in \Re^2$. In this work, the camera calibration parameters are defined in the focal plane (image space); therefore, the non-sharp tip image, due to the depth directional motion of the robot, is ignored. For an orthographic camera projection model, the tip position $^{S}\mathbf{p} = (X, Y, Z)^T$ in the slave frame is measured by a position encorder of the manipulator and can be related to its position $^{I}\mathbf{p}$ in an image space as follows:

$$^{I}\mathbf{p} = \begin{pmatrix} u \\ v \end{pmatrix} = \begin{pmatrix} \frac{X}{S_u} + u_0 \\ \frac{Y}{S_v} + v_0 \end{pmatrix} \tag{1}$$

where S_u and S_v are the pixel dimensions $(\mu\mathrm{m}/\mathrm{px})$ and the initial tip position $^{I}\mathbf{p}_0 = (u_0\ v_0)^T$ is measured by the template-matching method in the focal plane [16].

When assuming an accurately position-controlled micromanipulator and an orthographic projection model, it is important to initially locate the tip in the focal plane. In this work, the precise placement of the tip along the Z depth is achieved by the comparison of the pixel gradient magnitudes at the tip because the tip is angled and has pure translational motion. The gradient magnitudes are computed along the center line in the $\mathbf{u}$ direction of the tip, and the maximum values for each Z depth are compared. The gradient magnitude is at a maximum when the tip is in the focal plane.

B. Telerobotic Shared Control

The overall control architecture of the TSC system is described in Fig. 1. The TSC has two levels; the lower level consists of the direct manipulation and the autonomous controller based on an artificial potential field, and the higher level is the shared controller to integrate both modules. The total input command $^{S}\mathbf{u}$ for the micromanipulator is defined as the weighted sum of motion commands from the operator $(\mathbf{u}_h)$ and the autonomous controller $(\mathbf{u}_c)$

$$\begin{aligned} ^{S}\mathbf{u} &= K_h\mathbf{u}_h + K_c\mathbf{u}_c \\ K_h + K_c &= 1 \\ 0 \le (K_h, K_c) &\le 1 \end{aligned} \tag{2}$$

where K_h and K_c are the weighting factors for the operator and the controller, respectively.

The input from the human operator is the position command of the micromanipulator under position control: $\mathbf{u}_h = \alpha_p{}^{M}\mathbf{p}$, where $^{M}\mathbf{p}$ is the Cartesian tip position of a master device and α_p is the scaling factor. An artificial potential field-based control algorithm [22] is applied for the autonomous manipulation module, in which the manipulator is considered to be a particle and is controlled under a force field by attractive and repulsive potential functions. An attractive potential field is constructed to attract the manipulator to the guidance path, and a repulsive potential field is generated around a cell membrane to prevent the micropipette tip from passing the membrane in any direction other than the injection direction. The total potential field is defined by the sum of both potential fields, and each potential function is defined as follows:

$$\begin{aligned} U_{\mathrm{total}}(\mathbf{p}) &= U_{att}(\mathbf{p}) + U_{rep}(\mathbf{p}) \\ U_{\mathrm{att}}(\mathbf{p}) &= \frac{1}{2}K_a|\mathbf{p}_d - \mathbf{p}|^2 \\ U_{\mathrm{rep}}(\mathbf{p}) &= \frac{1}{2}K_r|\mathbf{p} - \mathbf{p}_o|^2, \quad \text{for } |\mathbf{p} - \mathbf{p}_o| \le r \end{aligned} \tag{3}$$

where $\mathbf{p}_d = \mathrm{nearest\ point}$ from the tip to the guidance path, $\mathbf{p}_o = \mathrm{nearest\ point}$ from the tip position to the membrane, K_a, $K_r = \mathrm{constant\ gains}$, and $r = \mathrm{radius\ of\ influence}$. The nearest points can be obtained from the closest point projection on the line path and the circle for the membrane. Finally, for the net force $\mathbf{f_p}$ is defined by the negative gradient of the potential field, and the input command from the artificial potential field algorithm is defined as: $\mathbf{u_c} = c_f\mathbf{f_p} = -c_f\nabla U_{total}$ where c_f is the compliance constant for modifying the input command in $\mu m/N$.

C. Shared Control Gain Tuning

In the TSC, the input commands from the direct manipulation module and the autonomous module to the shared controller have gains (weighting factors) of K_h and K_c, respectively. These gains play an important role in deciding which module will be weighted more in the TSC. High human operator weight can lead to the microinjection system acting as a conventional direct manipulation system. Conversely, when more weight is given to the automation module, the human operator can lose control of the micromanipulator.

In this work, to quantitatively evaluate the effect of the weighting level of each module on the TSC and so obtain the optimal gains, we performed 2D pointing and steering tasks based on Fitts' law and the steering law. Fitts' law and the steering law were first developed to quantify the speed and accuracy tradeoff in target-directed movements [23], [24]. They have been applied in various applications, such as human-computer interaction and robotics [25], [26].

In Fitts' law, the *Movement Time* (MT) in seconds to select a target of width W_f and at distance D_f is given by

$$MT = a + b\log_2\left(\frac{D_f}{W_f} + 1\right) \tag{4}$$

where a and b are empirical parameters determined by linear regression. The term $\log_2(D_f/W_f + 1)$ refers to the *Index of Difficulty* (ID) in *bits*, which represents the difficulties of the tasks.

In a typical Fitts' law formulation, the target-pointing movement is only considered between the initial and final positions, and it is thus not appropriate for trajectory-based tasks. Therefore, if the movement is constrained along a predefined path, the steering law accurately predicts the MT with path length D_s and width W_s [24]

$$MT = a + b\frac{D_s}{W_s}. \tag{5}$$

Although shared control between humans and robots has been widely studied and various applications for Fitts' law have been

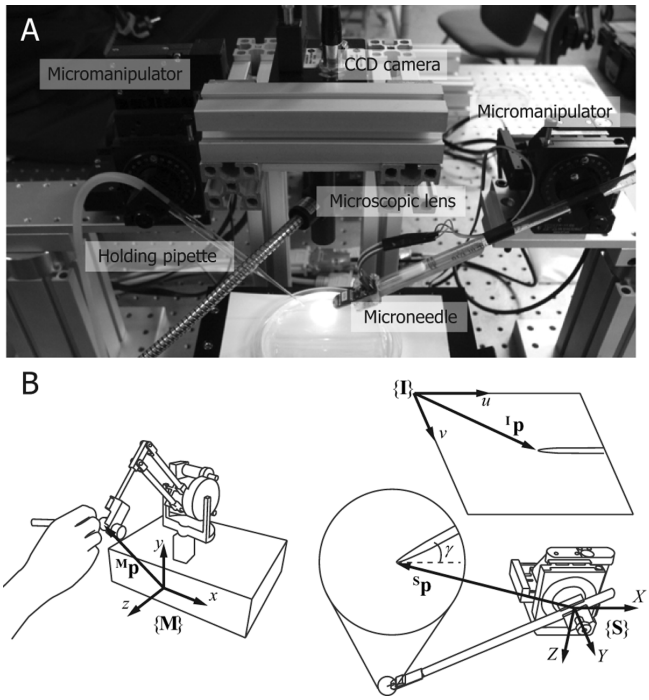

Fig. 2. (a) Experimental system setup and (b) coordinate frames. $\mathbf{p}$ is the position vector and γ is the injection angle of a slave tip in the Y direction.

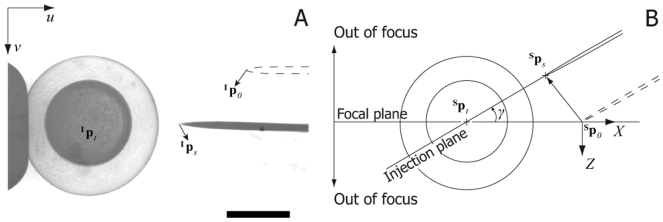

Fig. 3. (a) Captured image of a cell and (b) guidance path in the XZ plane. Subscript t is the target position in the yolk, and the green circle represents the edge detection of the yolk by the Hough transform. Subscripts 0 and s represent the initial point and the injection starting point, respectively. The guidance path is defined from ${}^{\mathrm{S}}\mathbf{p}_s$ to ${}^{\mathrm{S}}\mathbf{p}_t$. Scale bar is $500\ \mu m$.

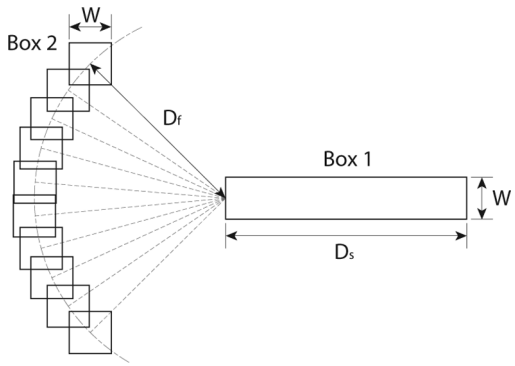

Fig. 4. The Fitts' and steering laws task window. Box 1 is the tunnel for the steering law task and box 2 is the target for the Fitts' law task. Both tasks have the same width but different amplitudes $W_f = W_s = W$.

presented, the quantitative analysis for choosing ideal weighting in shared control using Fitts' law has not been studied. Here, we present an experimental method for determining the ideal weights for shared control using Fitts' and steering law tests.

In the proposed TSC for microinjection, a micropipette-guiding task, i.e., directing the tip to a cell along the guidance path with depth directional motion compensation, can be seen as a steering law task, and target selection from the guidance path can be a Fitts' law task of compensating for target-detection error. We propose a model combining Fitts' law and the steering law, in which we hypothesized that the total index of difficulty ID_t (*bits*) is obtained by

$$MT = a + bID_t$$
$$ID_t = ID_f + d \cdot ID_s \tag{6}$$

where $ID_f = \log_2(D_f/W_f + 1)$ in (4) and $ID_s = D_s/W_s$ in (5), and d is $1 \cdot bits$ for unit conversion.

III. Experiment

A. System Setup

A biomicromanipulation workstation is shown in Fig. 2. Zebrafish embryos were used as suspended cells. The operator commanded the master robot (SensAble, PHANToM Premium 1.0, USA) to control the micromanipulator. The slave consists of a micromanipulator (PI, F-131, Germany) with an injection needle, and the other micromanipulator (Sutter, MP225, USA) with a holding glass pipette. The micromanipulators have three translational motions in the X, Y, and Z direction for input command $\mathbf{u}$ in μm. The vision system includes a CCD camera (SVS-Vistek, SVS340MUCP, Germany, 640×480) with a microscopic lens (Moritex, MML2-ST65D, $2 \times \mathrm{magnification}$). The position of the cell in the image space is extracted using the Hough transform as the center point of the detected circle, and the focusing of the nonangled holding pipette with a cell was implemented based on the template-matching method. Finally, the guidance path is determined as the linear path from the cell position to the injection starting position near the cell membrane, as shown in Fig. 3. The injection starting position ${}^{\mathrm{S}}\mathbf{p}_s$ is from ${}^{\mathrm{I}}\mathbf{p}_s$ located 40 px away from the cell contour edge. The gains for artificial potential field were set to $K_a = 1.0$, $K_r = 1.0$, and $c_f = 1.0$.

B. Fitts' and Steering Laws Test Design

Five participants (four males and one female aged 26.8 ± 2.2 years) participated in the experimental task. All participants were right-hand dominant and inexperienced in microinjection and teleoperation systems.

Fig. 4 shows the task window for the proposed model (6). The steering task was performed first for the tunnel (Box 1), in which the desired path was on the center line along the horizontal direction. The participants were asked to guide a white plus sign (${}^{\mathrm{I}}\mathbf{p}$) from the right side to the left side of the tunnel without crossing the top or bottom sides of the tunnel. The starting position of a white plus sign was randomly chosen every trial. After passing the tunnel, a square box appeared (Box 2), and the participants were instructed to put the plus sign on Box 2 and to click the button on the stylus of the haptic device. If the participants failed to perform the task by leaving the tunnel or mistargeting the square box, the white plus sign changed to a red plus sign, and the trial was restarted by positioning the tip in the starting position, reinitializing the timer. The completion time was recorded in *seconds* from the time of tunnel entry to the time of tapping Box 2, and the number of errors was also recorded. During the test, the participants were asked to perform the task as quickly as possible and were not informed on the principles of shared control.

Five gains ($K_h = 0.2, 0.4, 0.6, 0.8, 1.0$) were selected to compare the performance with different gains, and 15 total indices of difficulty (Table I) were selected. Each participant performed 10 sets of trials and each set consisted of 75 trials ($15\ \mathrm{IDt} \times 5\ \mathrm{gains}$) in random order.

TABLE I
TOTAL INDEX OF DIFFICULTY

W	D_s	D_f	ID_t	W	D_s	D_f	ID_t
40	50	90	2.95	30	180	90	8.00
30	50	95	3.73	30	200	90	8.67
40	100	80	4.08	20	150	90	9.96
20	50	80	4.82	20	180	80	11.32
40	200	70	6.46	10	90	90	12.32
30	150	80	6.87	10	100	70	13.00
20	100	70	7.17	10	120	50	14.58
10	50	40	7.32				

A

K_h	Model	r^2
○ 0.2	MT=0.6288+0.1133IDt	0.9317
× 0.4	MT=0.2837+0.1283IDt	0.8956
□ 0.6	MT=0.1786+0.1485IDt	0.9030
△ 0.8	MT= - 0.1224+0.2207IDt	0.8183
+ 1.0	MT= - 0.2864+0.2698IDt	0.9138

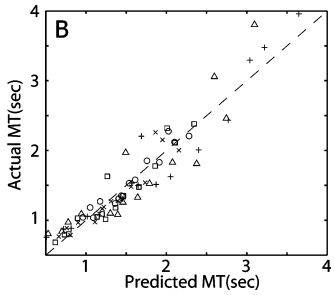

Fig. 5. (a) Linear regressions for TSC gains and (b) relationship between the actual and predicted values. The dashed line represents the unit slope for an ideal model.

Before the test, all of participants were performed the training set to become used to the teleoperation system. A total of 3750 trials were analyzed, excluding failed trials.

C. Results and Discussion

The experimental results along with the linear regression for the proposed model (6) are shown in Fig. 5. The experimental data fitted the model with an r^2 value over 0.8183, showing that the MTs were predicted well by the proposed model and that the model can thus be used for the performance measurement to evaluate the system and determine the TSC gains.

As a performance index for the comparison of system behavior with different gains, *throughput* (TP) was calculated [27], here defined as $TP = (1/m)\Sigma(1/n)\Sigma(ID_{tij}/MT_{ij})$ in *bits per second (bps)*, where $j = 1 : n$ is the number of trials and $i = 1 : m$ is the number of participants. TP is a useful measure for the speed and accuracy performance of movements by the integrated interpretation of the slope and intercept parameters of the regression model. The one-way within-subjects analysis of variance (ANOVA) test was used, and post-hoc analysis was performed using the Tukey's test. The ANOVA test showed a significant effect of the gains for TP $(p < 0.001)$, which indicated that the different TSC gains affected the task performance. Fig. 6(a) shows the TP values of the TSC gains. When $K_h = 0.2$, none of the participants performed better than other gains due to the strong constraints of the movements on the guidance path in performing the Fitts' targeting task. This meant that a greater weighting of the ability of the autonomous controller to control the manipulator hindered the operator's conscious actions to move the tip out of the guidance path to handle erroneous situations such as failed target detection, target movement during manipulation, and target occlusion by floating particles in the liquid medium. Conversely, a greater weighting on K_h means that more manipulation capability is given to the operator; when $K_h = 1.0$, the manipulation is the same as with the direct manipulation mode (no intervention of the controller). In the direct manipulation, the participants easily strayed from the guidance path in performing the steering task and had a lower TP.

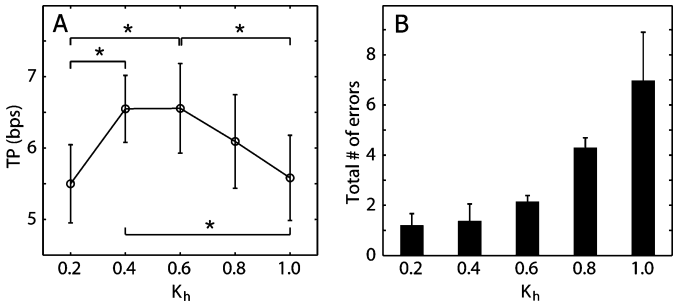

Fig. 6. (a) TP and (b) number of errors during the task execution for TSC gains $(*p < 0.05)$.

Fig. 6(b) shows the total number of errors for all trials $(F_{4,12} = 30.4476,\ p < 0.001)$. As defined above, the error was counted when the tip failed to track the guidance path (steering law) or in pointing to the target (Fitts' law). For higher K_h, the accuracy was lower due to weak constraints on the guidance path, and the direct manipulation showed a larger number of errors during the manipulation. In addition, as shown in Fig. 5, higher K_h values led to an increase in the slope of the regression model. This indicated that there was relatively smaller performance difference at higher K_h between a low-ID_t task and a high-ID_t task. In other words, the intervention of the autonomous controller reduced the influence of operator skill in performing the manipulation task.

The participants showed the best performance at K_h values of 0.4 and 0.6, with higher TP values and a lower number of errors (there was statistically no significant difference between $K_h = 0.4$ and $K_h = 0.6$ in TP and the number of errors). This range thus represents the optimal gain of the TSC for the microinjection task, and the TSC showed better results than direct manipulation. Some level of automation or human involvement was needed in the development of the robotic biomicromanipulation system from the standpoint of speed and accuracy performance.

In this study, the evaluation for $K_h = 0$ could not be given because it was impossible to perform the Fitts' targeting task; the operator could only control the manipulator in the guidance path. Although the fully automated system or the intervention of the autonomous function in telemanipulation could enhance microinjection performance by reducing human deficiencies, as the weight of the controller was increased, the operators lost their ability to control the manipulator's motion. Microinjection is a tedious task requiring much skill and practice to manipulate tiny cells with delicate glass tools, which requires cell separation, selection, targeting, tracking and multi DOF manipulation. Therefore, the loss of control ability is problematic for this complicated task. In addition, automatic dexterous manipulation including the rotation of cells has not yet been reported, and there are difficulties in target selection in visual processing. Jang *et al.* [11] reported that the failed recognition rate in the worst case was 47.8% for the detection of the nucleus and the polar body of mouse embryos. In [12] and [13], approximately 15% of the attached cells (CHO-K1 and endothelial cells, respectively) were missed in the visual targeting process.

IV. CONCLUSION

In the context of the single-cell microinjection system, we proposed a TSC to achieve simultaneously high throughput and dexterity. In particular, for the evaluation of TSCs with different gains, the microinjection task was modeled through the Fitts' and steering laws. The results showed that a 40–60% weighting on the human operator (or the controller) produced better performance for both speed and accuracy of the guiding and targeting task in microinjection. In addition, the pro-

posed evaluation method provides a theoretical basis for the selection of shared control gain in as system requiring the simultaneous achievement of high throughput and dexterity. The design of the optimal control weights on a human operator and a robot is the most challenging issue for the shared control area. The weighting can be different depending on the application of the shared control concept, for which the proposed method can be used to quantitatively evaluate performance via the modeling of other manipulation tasks of interest using Fitts' and steering laws.

In future work, TSC design for the whole task in microinjection and experiment with biological samples will be performed. In addition, the proposed method will be applied to other cell manipulation applications.

REFERENCES

[1] D. Luo and W. M. Saltzman, "Synthetic DNA delivery systems," *Nature Biotechnol.*, vol. 18, pp. 33–37, Jan. 2000.

[2] D. J. Stephens and R. Pepperkok, "The many ways to cross the plasma membrane," *Proc. Nat. Acad. Sci. United States of America*, vol. 98, pp. 4295–4298, Apr. 2001.

[3] Y. Zhang and L. C. Yu, "Microinjection as a tool of mechanical delivery," *Current Opinion in Biotechnol.*, vol. 19, pp. 506–510, Oct. 2008.

[4] J. K. Valley *et al.*, "Parallel single-cell light-induced electroporation and dielectrophoretic manipulation," *Lab. Chip*, vol. 9, pp. 1714–1720, 2009.

[5] U. K. Tirlapur and K. Konig, "Cell biology—Targeted transfection by femtosecond laser," *Nature*, vol. 418, pp. 290–291, Jul. 2002.

[6] H. J. Kim *et al.*, "Ultrasound-mediated transfection of mammalian cells," *Human Gene Therapy*, vol. 7, pp. 1339–1346, Jul. 1996.

[7] X. Liu *et al.*, "Automated microinjection of recombinant BCL-X into mouse zygotes enhances embryo development," *Plos One*, vol. 6, no. 7, 2011.

[8] H. B. Huang *et al.*, "Visual-based impedance control of out-of-Plane cell injection systems," *IEEE Trans. Autom. Sci. Eng.*, vol. 6, no. 3, pp. 565–571, Jul. 2009.

[9] Y. Xie *et al.*, "A force control approach to a robot-assisted cell microinjection system," *Int. J. Robot. Res.*, vol. 29, no. 9, pp. 1222–1232, Aug. 2010.

[10] P. Kallio *et al.*, "Injection guidance system for cellular microinjections," *Int. J. Robot. Res.*, vol. 26, no. 11–12, pp. 1303–1313, Nov./Dec. 2007.

[11] M. S. Jang *et al.*, "Shape recognition of the embryo cell using deformable template for micromanipulation," *Innovations in Appl. Artif. Intell.*, vol. 3029, pp. 463–472, 2004.

[12] G. Becattini *et al.*, "Diffusion tensor driven contour closing for cell microinjection targeting," in *Proc. IEEE EMBS*, Buenos Aires, Argentina, 2010, pp. 4072–4075.

[13] W. H. Wang *et al.*, "Machine vision and image processing for automated cell injection," in *Proc. IEEE/ASME Int. Conf. Mech. Embed. Syst. Appl.*, Beijing, China, 2008, pp. 309–314.

[14] M. Ammi *et al.*, "Evaluation of 3D pseudo-haptic rendering using vision for cell micromanipulation," in *Proc. IEEE/RSJ Int. Conf. Intell. Robot. Syst.*, Beijing, China, 2006, pp. 2115–2120.

[15] A. Pillarisetti *et al.*, "Evaluating the effect of force feedback in cell injection," *IEEE Trans. Autom. Sci. Eng.*, vol. 4, no. 3, pp. 322–331, Jul. 2007.

[16] J. Kim *et al.*, "A haptic interaction method using visual information and physically based modeling," *IEEE/ASME Trans. Mechatronics*, vol. 15, pp. 636–645, 2010.

[17] A. Bettini *et al.*, "Vision-assisted control for manipulation using virtual fixtures," *IEEE Trans. Robot. Autom.*, vol. 20, no. 6, pp. 953–966, Dec. 2004.

[18] W. B. Griffin *et al.*, "Feedback strategies for telemanipulation with shared control of object handling forces," *Presence-Teleoperators and Virtual Environments*, vol. 14, pp. 720–731, Dec. 2005.

[19] M. Ammi and A. Ferreira, "Involving the operator in the control strategy for intelligent telemicromanipulation," in *Proc. IEEE/ASME Int. Conf. Adv. Intell. Mech.*, 2003, pp. 868–873.

[20] Z. Y. Zhang, "A flexible new technique for camera calibration," *IEEE Trans. Pattern Anal. Mach. Intell.*, vol. 22, no. 11, pp. 1330–1334, Nov. 2000.

[21] M. Ammi *et al.*, "Automatic camera-based microscope calibration for a telemicromanipulation system using a virtual pattern," *IEEE Trans. Robot.*, vol. 25, no. 1, pp. 184–191, Feb. 2009.

[22] O. Khatib, "Real-time obstacle avoidance for manipulators and mobile robots," *Int. J. Robot. Res.*, vol. 5, pp. 90–98, Spr. 1986.

[23] P. M. Fitts, "The information capacity of the human motor system in controlling the amplitude of movement," *J. Exp. Psychol.*, vol. 47, pp. 381–391, Jun. 1954.

[24] J. Accot and S. Zhai, "Beyond Fitts's law: Models for trajectory-based HCI tasks," *CHI*, pp. 295–302, 1997.

[25] O. Tonet *et al.*, "Control of a teleoperated nanomanipulator with time delay under direct vision feedback," in *Proc. IEEE Int. Conf. Robot. Autom.*, Roma, Italy, 2007, pp. 3514–3519.

[26] C. Choi *et al.*, "Development and quantitative performance evaluation of a noninvasive EMG computer interface," *IEEE Trans. Biomed. Eng.*, vol. 56, no. 1, pp. 188–191, Jan. 2009.

[27] R. W. Soukoreff and I. S. MacKenzie, "Towards a standard for pointing device evaluation, perspectives on 27 years of Fitts' law research in HCI," *Int. J. Human-Computer Studies*, vol. 61, pp. 751–789, Dec. 2004.

Seam Following for Automated Industrial Fiber Mat Stitching

Mario Richtsfeld, *Student Member, IEEE*, and Markus Vincze, *Member, IEEE*

***Abstract*—This paper presents a method for automatic seam following of two overlapping carbon fiber mats based on laser scans. We introduce a novel approach that combines one existing and two newly developed edge detection methods in a two out of three voting scheme to obtain high edge tracking robustness. The experimental results demonstrate the feasibility of a fully automated, sensor-guided robotic stitching process. The seam can be located within 1.0 mm at a detection rate of 99.3%.**

***Note to Practitioners*—This paper was motivated by the problem of stitching carbon fiber mats with an autonomously guided robot to realize the production of carbon fiber mats in lot-size one. Existing approaches use manually programmed robots, which following the seam of the material draped of preforms. This is time consuming and not suited for a production of many different parts at very low numbers. For the application continuous edge tracking and real-time performance must be guaranteed to obtain a continuous stitching process.**

***Index Terms*—Range sensing, recognition, visual tracking.**

I. INTRODUCTION

Today, automobile and aeronautics industry increasingly use robust and light weight parts made of Carbon Fiber Reinforced Polymer (CFRP). Besides the mechanical properties, CFRP elements have the advantage of integrating external elements easily into the CFRP elements due to the specific production process. Several different

Manuscript received May 02, 2011; revised August 11, 2011; accepted November 06, 2011. Date of publication December 01, 2011; date of current version April 03, 2012. This paper was recommended for publication by Associate Editor S. Zhou and Editor V. Kumar upon evaluation of the reviewers' comments.

The authors are with the Automation and Control Institute (ACIN), Vienna University of Technology, Gusshausstrasse 27-29 / E376, A-1040 Vienna, Austria (e-mail: richtsfeld@acin.tuwien.ac.at; vincze@acin.tuwien.ac.at).

Color versions of one or more of the figures in this paper are available online at http://ieeexplore.ieee.org.

Digital Object Identifier 10.1109/TASE.2011.2175917